Journal of Molecular Structure 1284 (2023) 135312

Contents lists available at ScienceDirect

Journal of Molecular Structure

journal homepage: www.elsevier.com/locate/molstr

Analysis of boronic acids containing amino ferrocene by DFT approach and in silico studies

Usman Sani Muhammad[a], Sultan Erkan[a,*], Savaş Kaya[b]

[a] Department of Chemistry, Faculty of Science, Sivas Cumhuriyet University, Sivas, Tukey
[b] Department of Pharmacy, Vocational School of Health Services, Sivas Cumhuriyet University, Sivas 58140, Turkey

ARTICLE INFO

Article history:
Received 20 July 2022
Revised 20 February 2023
Accepted 23 February 2023
Available online 7 March 2023

Keywords:
Ferrocene
DFT
NLO
OLED
Molecular docking

ABSTRACT

The synthesized (2)-(6) complexes and (2′)-(6′) hypothetical complexes formed by attached boranic acid esters were optimized at the DFT-B3LYP/GEN level. The structural and spectroscopic properties (IR, ^{1H}NMR , ^{13C}NMR) of the optimized complex structures were calculated and the complexes were characterized. Molecular orbital energy diagrams and some molecular properties of the complexes were calculated. Some quantum chemical parameters were calculated for the biological activities of the complexes. It was predicted that complexes with diboranic acid ester had higher biological abilities. They were docked against Burkitt's lymphoma (BL) cell line for their anticancer activities and similar trend was obtained with quantum chemical parameters. NLO and OLED properties were examined to evaluate the electronic properties of the complexes. These properties of the complexes were found to be advantageous over the related reference materials.

1. Introduction

Organometallic compounds are studied in pharmaceutical chemistry because of their biologically activating properties [1]. Ferrocene (iron complexes with bis(η^5-cyclopentadienyl) ligand) forms an important part of the compounds with the biomedical properties of organometallic chemistry [2]. Ferrocene compounds have analgesic, antineoplastic, anticonvulsant, anti-HIV, antitumor, antimalarial, antioxidant, antimicrobial and DNA fragmentation activities [3]. Especially these organometallic compounds are considered as important agents in cancer treatment. Evidence of this is seen in drugs containing ferrocifen, tamoxifen and ferroquine [4] substituents used in cancer treatment. In addition to medical applications of ferrocene compounds, their photochemical stability and industrial use are among the applications that cannot be ignored [5]. Ferrocene-based organomatalic compounds, which were used for the first time in the treatment of breast cancer, also achieved successful results in colon and liver cancer [6]. Moreover, many organometallic molecular π-delocalized systems are notable for their significant non-linear optical (NLO) and organic light-emitting diode (OLED) properties resulting from their push-pull structures. In addition, there are boronic acid derivatives that are not toxic to the human body, such as ferrocene [7–13]. Boronic acid-based drugs are particularly tumor-targeting [14]. Therefore, boronic acids are one of the drugs actively used in the treatment of blood cancers developing in the bone marrow [15–17]. In addition to the medical applications of boron compounds, it also has rich application areas as production storage and electrolyte materials [18]. Ferrocene-containing boronic acids can affect covalent interactions in biomolecules and moreover, redox-controlled oscillations in electrochemical applications. This can lead to the dissolution of non-polar molecules in the biological domain in aqueous media and increase their drug-carrying ability [19].

Mokhir et al. investigated the anticancer properties of aminoferrocene-based prodrug (2)-(6) [20].

In this study, in addition to the synthesized ferrocene boranic acids ((2), (3), (4), (5), (6)), hypothetical ferrocene diboranic acids ((2′), (3′), (4′), (5′), (6′)) were handled by computational chemistry methods. The molecular structures of the studied complexes are shown in Scheme 1. The studied complexes were optimized by the B3LYP method of the Density function theory (DFT) method. All complexes are structurally determined by spectroscopic methods (IR and NMR). NMR and IR spectroscopic data is suggested for all complexes with the calculation level B3LYP/GEN. The electronic properties of the studied complexes are estimated from the frontier molecular orbital (HOMO and LUMO) contour diagrams. Total static dipole moment (μ), mean linear polarizability (α), polarizability anisotropy ($\Delta\alpha$) and first hyperpolarizability (β) parameters were calculated to estimate the NLO properties of the complexes. The OLED performances of the complexes were predicted

* Corresponding author.
E-mail address: sultanerkan@cumhuriyet.edu.tr (S. Erkan).

https://doi.org/10.1016/j.molstruc.2023.135312
0022-2860/

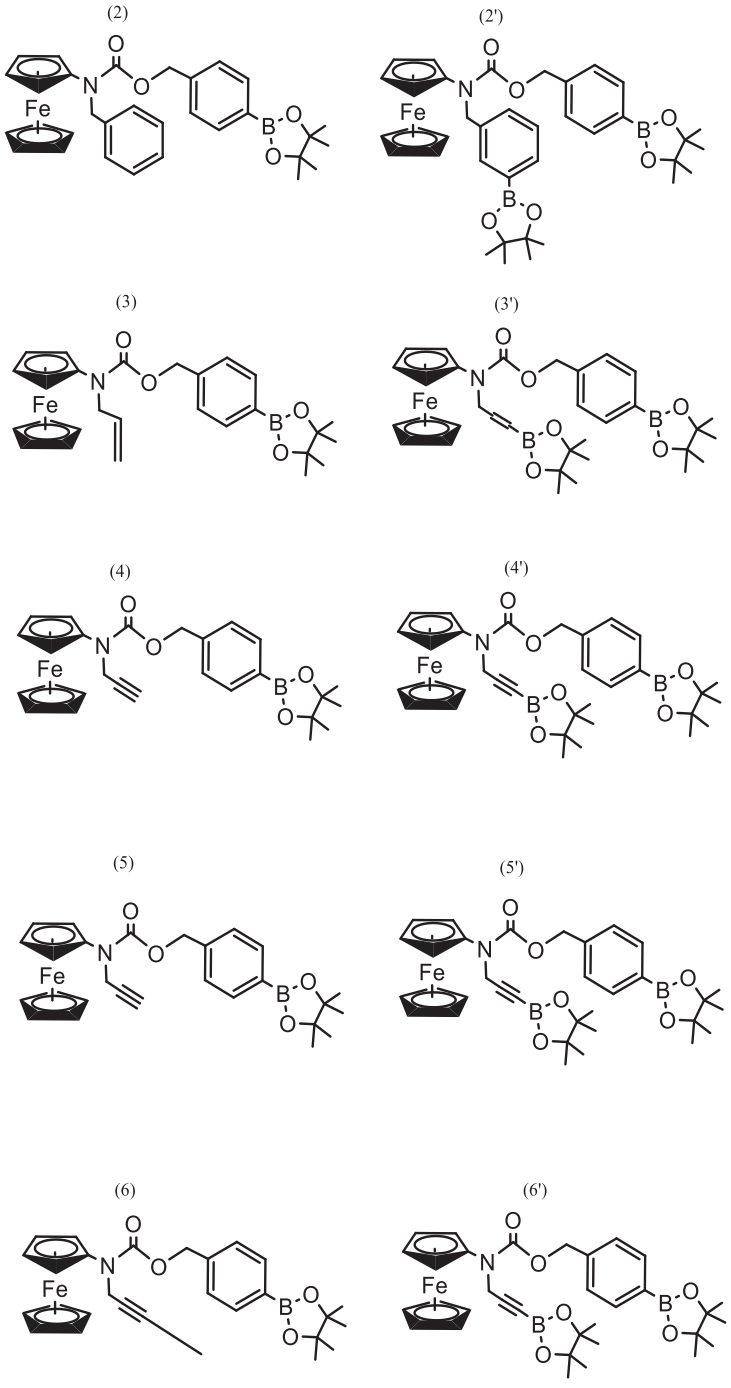

Scheme 1. 2D-Structure of the studied ferrocene complexes.

from the electron transport layer (ETL), hole transport layer (HTL), electron injection layer (EIL) and hole injection layer (HIL) parameters. Finally, PDB ID: 3C0R, representing a rare malignancy originating from B cells, Burkitt's lymphoma (BL), was docked onto the target protein with the aid of a simulation.

2. Calculation methods

The molecular structures of the investigated ferrocene complexes were designed in GaussView 6.0.16 program [21]. The optimized structures and vibrational frequencies of the complexes were obtained at the DFT-B3LYP/GEN level in the Gaussian 09:AS64L-G09RevD.01 program [22]. LANL2DZ/6–31 G is a mixed basis set [23,24]. NMR spectra were performed using the indicator-free atomic orbitals (GIAO) method [25]. Molecular docking has been implemented in HEX 8.0.0 [26].

3. Result and discussion

3.1. Optimized structure

Synthesized ((2), (3), (4), (5), (6)) and their hypothetical boranic acid esters ((2′), (3′), (4′), (5′), (6′)) optimized at DFT-B3LYP/GEN level (LANL2DZ for iron atom and 6–31 G for other atoms). As a result of the frequency calculations, the imaginary frequency was

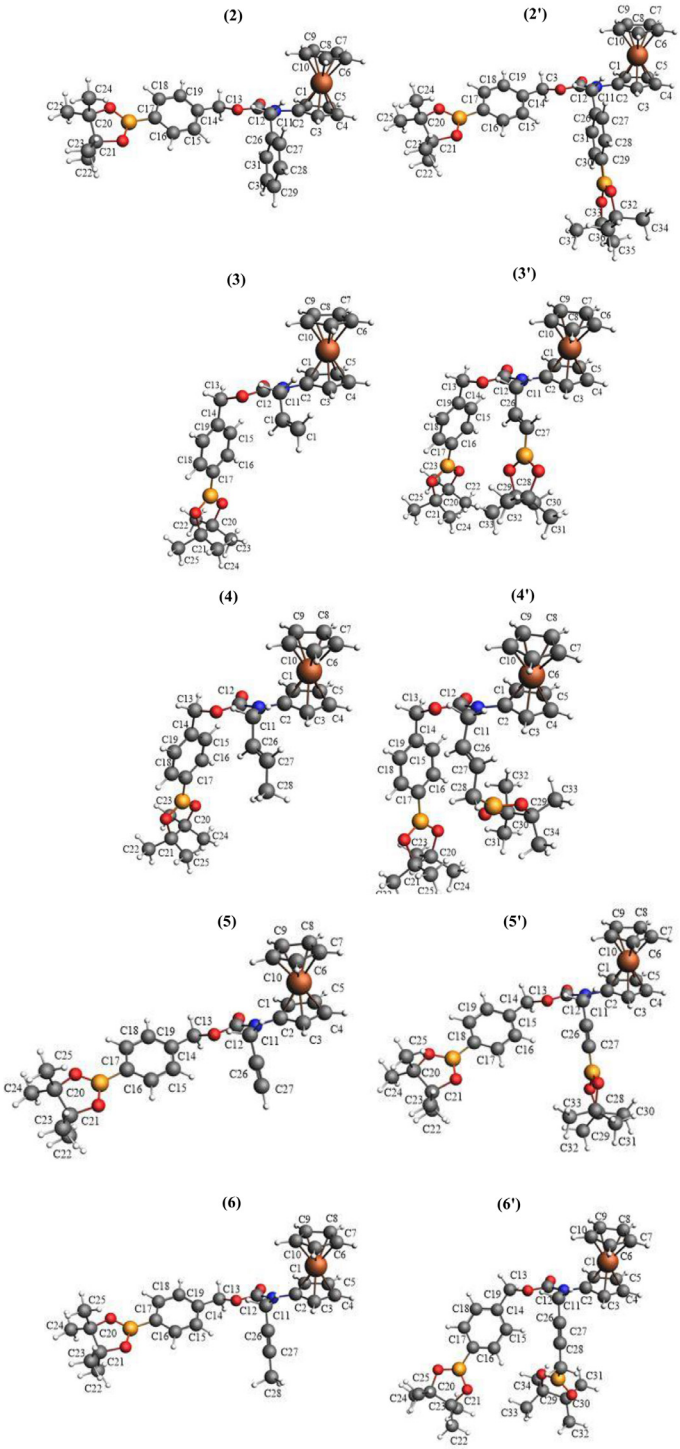

Fig. 1. Optimized structure ferrocene boranic acid complexes.

found to be 0. Three-dimensional structures positioned at the lowest energy position in space by optimization are given in Fig. 1.

According to the geometric structures obtained, the cyclopentadienyl ligand is a five-electron donor to the metal atom and the ferrocene structure has an eclipsed orientation "sandwich" structure located in the D_{5h} point group. The bond lengths between the carbon atoms of the pentahaptocyclopentadienyl ligand are identical to each other and the bond lengths between the carbon atoms are 1.43 Å and bond angles are approximately 107°.

Substituent change of synthesized complexes takes place over the nitrogen atom. Considering the importance of boron compounds in the literature in recent years [27,19,28], the advantages of diboranic acid should be evaluated. For complex (2), the distance between boron and oxygen bonds is 1.39 Å and the bond angle (OBO) is 111.5°. The boranic acid substituents added in the hypothetical complex (2′) have the same bond lengths and bond angles as in the (2) complex. Similar results were obtained when comparing other complexes.

3.2. The harmonic vibration frequencies and labeling of the peaks

DFT methods in polyatomic molecules provide more accurate results in spectral analysis techniques [29]. Harmonic frequencies are given in the infrared spectra obtained by DFT methods [30]. The vibration spectra of the studied complexes, including the experimentally synthesized complexes ((2), (3), (4), (5), (6)) are not available in the literature. It is very difficult to read the IR spectra of ferrocene complexes with polyatomic and complex structures. In addition, labeling in the IR spectra of hypothetical complexes will provide important information for future studies of ferrocene complexes. For this purpose, IR spectra calculated with DFT/B3LYP/LANL2DZ-6–31 G level of the synthesized and hypothetical ferrocene complexes are given in Fig. 2. The detailed analysis of the modes given in Fig. 2 is given in Table 1. The relationship of the peaks with the highest densities of the studied complexes with the molecular structure was investigated.

In general, the highest frequency among the obtained spectra belongs to the C–H bond stretching. The lowest frequency is the Fe-C bond stretching vibration belonging to the ferrocene group in the fingerprint region in the range of 440–470 cm^{-1}. After the high-frequency C–H bond stretching, the peaks generally show C = O bond stretching at approximately 1700 cm^{-1}. Another specific peak is the C = C bond stretching at 1400 cm^{-1}. In the spectrum given in Fig. 2, there are bending regions in two regions. These vibrational stretching are caused by the angular change of the ligaments. Generally, there are combinations such as rocking, wagging and scissoring in the bending region resulting from the movement of hydrogen atoms.

In the spectrum given in Fig. 2, 13 frequency labels have been made for complex (2). The first spectrum is the bond stretching frequency at 3285 cm^{-1} and belongs to the ferrocene carbon-hydrogen bond stretching as in all complexes. Spectrum with number 2 is 3217 cm^{-1} and corresponds to aromatic carbon-hydrogen bond stretching. The bond stretching of the aliphatic carbon-hydrogen bond is seen as two peaks and these peaks mark the 2nd and 3rd regions in the spectrum. In this region, the frequencies at 3140 and 3064 cm^{-1} belong to the νC_{ali}-H vibrational frequencies of boronic acid substituents. The frequency at 1696 cm^{-1} has a high peak intensity and belongs to the C = O bond stretching mode. Region 5 in Fig. 2 is the bending region of molecular vibrations that occur with the change of angles and hydrogen atoms make stretching such as scissoring, rocking, wagging, twisting. The boron-carbon bond vibrational frequency is 1398 cm^{-1} and corresponds to the 6th region in the spectrum. 7 and 8 peaks are C = C and C–C bond stretching vibrations and their frequencies are 1356.6 and 1307.2 cm^{-1}, respectively. In addition to the bending of hydrogen atoms at 1268 cm^{-1}, it is C–N bond stretching. The peaks numbered 10 and 11 in the spectrum correspond to the B-O and C–O bond stretching's at 1137 and 1089 cm^{-1}, respectively. Mode 12 is the bending zone. Finally, the last peak belongs to ferrocene and is the iron-carbon bond stretching at 427 cm^{-1}. The same bond stretching was obtained in similar regions for the other complexes. The only difference is the specific number 4 peak C≡C bond stresses for the 5, 5′, 6 and 6′ complexes.

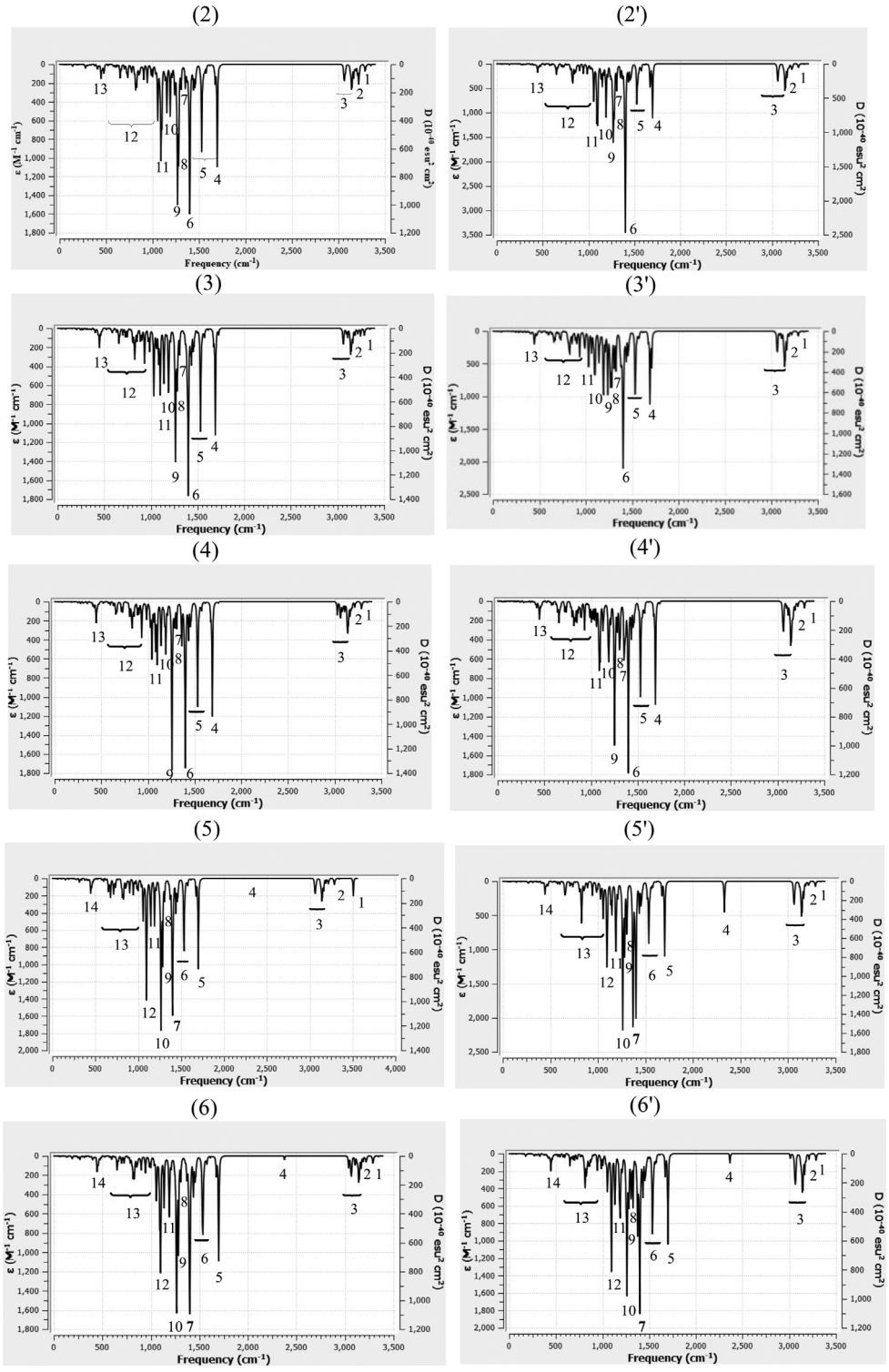

Fig. 2. Calculated FT-IR spectrums of investigated ferrocene complexes.

3.3. ^{13}C and ^{1H}NMR chemical shift

NMR spectra of molecules can be calculated by computational chemistry methods. NMR was calculated as the work type for the studied complexes, and GIAO (Gauge-Independent Atomic Orbital) [31] and DFT-B3LYP/GEN levels were calculated as the method. The ^{13C}NMR chemical shift values of the ferrocene complexes are given in Tables 3 and 4 by taking the difference between the absolute shielding values of the sample and the reference. ^{13C}NMR chemical shifts of the complexes were performed considering the basic skeletal structures of the complexes. The complexes were evaluated separately on the basis of three different skeletons as ferrocene, aromatic, aliphatic and boronic acid esters. ^{1H}NMR chemical shifts are given in Tables S1 and S2 in the Sup. Met. section. Chemical shifts are given relative to the TMS reference. The shielding for the TMS proton in the gas phase was found to be 32.77 ppm and for the carbon 194.41 ppm. ^{1H}NMR and ^{13C}NMR chemical shift values of investigated complexes were calculated

Table 1
Infrared frequencies in cm-1 and assignments of (2), (3), (4), (5) and (6) complexes.

Mod	(2)	Ass.	(3)	Ass.	(4)	Ass.	(5)	Ass.	(6)	Ass.
1	3285.7	ν_{C-H}	3285.7	ν_{C-H}	3285.9	ν_{C-H}	3285.6	ν_{C-H}	3285.6	ν_{C-H}
2	3217.7	ν_{C-H}	3216.4	ν_{C-H}	3215.4	ν_{C-H}	3217.0	ν_{C-H}	3216.8	ν_{C-H}
3	3140.1–3064.5	ν_{C-H}	3140.4–3055.7	ν_{C-H}	3140.1–3028.5	ν_{C-H}	3140.4–3064.6	ν_{C-H}	3140.3–3064.6	ν_{C-H}
4	1696.1	$\nu_{C=O}$	1690.2	$\nu_{C=O}$	1688.8	$\nu_{C=O}$	2235.3	$\nu_{C\equiv C}$	2375.7	$\nu_{C\equiv C}$
5	1674.1–1440.0	Bend.	1672.4–1422.4	Bend.	1672.5–1434.6	Bend.	1700.1	$\nu_{C=O}$	1698.4	$\nu_{C=O}$
6	1398.3	ν_{B-C}	1400.4	ν_{B-C}	1400.1	ν_{B-C}	1673.8–1437.7	Bend.	1673.8–1437.3	Bend.
7	1356.6	$\nu_{C=C}$	1361.1	$\nu_{C=C}$	1360.5	$\nu_{C=C}$	1401.5	ν_{B-C}	1401.3	ν_{B-C}
8	1307.2	ν_{C-C}	1307.0	ν_{C-C}	1307.5	ν_{C-C}	1355.0	$\nu_{C=C}$	1354.3	$\nu_{C=C}$
9	1268.5	ν_{C-N}	1263.2	ν_{C-N}	1257.3	ν_{C-N}	1307.0	ν_{C-C}	1307.4	ν_{C-C}
10	1137.1	ν_{B-O}	1137.6	ν_{B-O}	1137.1	ν_{B-O}	1263.5	ν_{C-N}	1262.6	ν_{C-N}
11	1089.7	ν_{C-O}	1082.4	ν_{C-O}	1081.4	ν_{C-O}	1137.0	ν_{B-O}	1136.3	ν_{B-O}
12	1029.5–480.5	Bend.	1060.0–523.0	Bend.	1042.1–520.7	Bend.	1095.0	ν_{C-O}	1090.9	ν_{C-O}
13	472.9	ν_{C-Fe}	447.6	ν_{C-Fe}	445.0	ν_{C-Fe}	1060.3–521.8	Bend.	1054.3–516.5	Bend.
14	–	–	–	–	–	–	445.9	ν_{C-Fe}	444.9	ν_{C-Fe}

Table 2
Infrared frequencies in cm-1 and assignments of (2′), (3′), (4′), (5′) and (6′) complexes.

Mod	(2′)	Ass.	(3′)	Ass.	(4′)	Ass.	(5′)	Ass.	(6′)	Ass.
1	3285.9	ν_{C-H}	3285.8	ν_{C-H}	3285.9	ν_{C-H}	3285.6	ν_{C-H}	3285.9	ν_{C-H}
2	3216.5	ν_{C-H}	3188.5	ν_{C-H}	3217.6	ν_{C-H}	3216.1	ν_{C-H}	3112.3	ν_{C-H}
3	3140.5–3064.9	ν_{C-H}	3140.2–3064.4	ν_{C-H}	3140.0–3064.2	ν_{C-H}	3140.5–3065.2	ν_{C-H}	3139.8–3064.2	ν_{C-H}
4	1697.6	$\nu_{C=O}$	1690.1	$\nu_{C=O}$	1689.9	$\nu_{C=O}$	2330.2	$\nu_{C\equiv C}$	2364.9	$\nu_{C\equiv C}$
5	1673.7–1445.8	Bend	1672.6–1445.1	Bend	1672.0–1445.7	Bend	1702.3	$\nu_{C=O}$	1700.8	$\nu_{C=O}$
6	1401.7	ν_{B-C}	1400.5	ν_{B-C}	1400.0	ν_{B-C}	1673.5–1445.5	Bend	1671.4–1445.4	Bend
7	1354.8	$\nu_{C=C}$	1361.3	$\nu_{C=C}$	1359.5	$\nu_{C=C}$	1400.7	ν_{B-C}	1399.8	ν_{B-C}
8	1307.3	ν_{C-C}	1306.9	ν_{C-C}	1308.6	ν_{C-C}	1353.8	$\nu_{C=C}$	1351.2	$\nu_{C=C}$
9	1268.7	ν_{C-N}	1266.2	ν_{C-N}	1266.0	ν_{C-N}	1306.9	ν_{C-C}	1307.2	ν_{C-C}
10	1136.8	ν_{B-O}	1137.6	ν_{B-O}	1136.1	ν_{B-O}	1261.2	ν_{C-N}	1261.2	ν_{C-N}
11	1090.9	ν_{C-O}	1092.6	ν_{C-O}	1089.1	ν_{C-O}	1136.7	ν_{B-O}	1138.3	ν_{B-O}
12	1057.1–516.9	Bend	1034.5–513.5	Bend	1036.9–517.8	Bend	1094.5	ν_{C-O}	1095.0	ν_{C-O}
13	445.3	ν_{C-Fe}	443.9	ν_{C-Fe}	447.3	ν_{C-Fe}	1036.3–518.6	Bend	1034.9–515.3	Bend
14	–	–	–	–			443.9	ν_{C-Fe}	445.9	ν_{C-Fe}

from the relation $\delta=\Sigma_{TMS}-\Sigma$ [32]. Here, Σ_{TMS} is the shielding of the TMS proton or carbon, and Σ is the shielding of the carbon or proton in the sample.

When Tables 3 and 4 are examined, it is seen that (2)-(6) and (2′)-(6′) complexes contain equivalent carbons and protons. Carbons and protons in opposite positions are replaced by a rotation process. Therefore, they are equivalent atoms. Equivalent atoms peak at the same chemical shift. The experimental ^{13}C and ^{1H}NMR chemical shifts for the (2)-(6) complex are in good agreement with the experimental results. For the (3) complex, the experimentally chemical shift value of the carbon atom at 154.52 pm was calculated as 154.68 ppm with the DFT-B3LYP/GEN level and it was determined that it belongs to the carbon atom number 12. The carbon chemical shift at 139 ppm is for carbon 14 and the calculated result is 135 ppm. When the results are evaluated one by one, the experimental values and the calculation results are close to each other. In general, the studied complexes appear to have high chemical shift values of carbons adjacent to nitrogen and oxygen. In this situation, the fact that the carbon atom is adjacent to the nitrogen and oxygen atoms with high electronegativity caused these protons to be less shielded and to have a high ppm value. The aliphatic carbon atoms have been calculated to have a low ppm value. Because these atoms do not feel the inductive effect of electronegative atoms. For these reasons, their nuclei are highly shielded by their electrons and they peak at low ppm. This is spectroscopically important for atomic labeling in the NMR spectra of hypothetical complexes. It should also be noted that the boranic acid ester ligand has an electron-attracting effect on the C26 and C27 carbons. In general, the designed complexes can be evaluated in terms of chemical and biological change by adding an electronegative ligand.

3.4. Quantum chemical parameters

In Table 5, the calculated values of the quantum chemical parameters of the ((2)-(6) and (2′)-(6′)) complexes are given. Calculations are made in the gas phase at the B3LYP/GEN level. Quantum chemical parameters such as highest occupied molecular orbital energy (E_{HOMO}) and lowest unoccupied molecular orbital energy (E_{LUMO}) are the chemical parameters that are mostly used. The way molecules interact with other species is determined by these orbitals, also known as boundary orbitals [33]. The ways of obtaining quantum chemical parameters are given in Eqs. (1)-(8).

$$I = -E_{HOMO} \tag{1}$$

$$A = -E_{LUMO} \tag{2}$$

$$\eta = \frac{1}{2}\left[\frac{\partial^2 E}{\partial^2 N}\right]_{\nu(r)} = \frac{I-A}{2} \tag{3}$$

$$\langle\alpha\rangle = \frac{1}{3}[\alpha_{xx}+\alpha_{yy}+\alpha_{zz}] \quad \sigma = \frac{1}{\eta} \tag{4}$$

$$\mu = -\chi = \left[\frac{\partial E}{\partial N}\right]_{\nu(r)} = -\left(\frac{I+A}{2}\right) \tag{5}$$

$$\omega = \frac{\chi^2}{2\eta} \tag{6}$$

$$\varepsilon = \frac{1}{\omega} \tag{7}$$

$$\omega^+ = \frac{(I+3A)^2}{16(I-A)} \quad \omega^- = \frac{(3I+A)^2}{16(I-A)} \tag{8}$$

From our result, we can see the high value of E_{HOMO} in molecules with boronic acid derivative (2,3,4,5 and 6) while E_{HOMO}

Table 3
^{13C}NMR chemical shift values (ppm) of (2)-(6) complexes.

(2)	δ	(3)	δ	(4)	δ	(5)	Δ	(6)	δ
Ferrocene Carbons									
C1	65.19	C1	66.92	C1	66.64	C1	66.24	C1	66.35
C2	101.11	C2	101.70	C2	101.79	C2	100.89	C2	100.99
C3	59.75	C3	58.29	C3	58.15	C3	58.42	C3	58.60
C4	64.73	C4	64.43	C4	64.31	C4	64.34	C4	64.66
C5	66.43	C5	65.81	C5	65.89	C5	65.96	C5	66.49
C6	68.37	C6	68.47	C6	69.69	C6	69.92	C6	69.63
C7	69.39	C7	69.36	C7	68.35	C7	68.57	C7	68.31
C8	69.52	C8	69.37	C8	68.81	C8	69.01	C8	69.26
C9	70.52	C9	70.42	C9	70.31	C9	70.29	C9	70.28
C10	71.39	C10	71.05	C10	71.15	C10	71.25	C10	71.39
Aromatic Carbons									
C14	135.15	C14	135.99	C14	136.10	C14	135.85	C14	135.70
C15	123.04	C15	126.64	C15	126.85	C15	126.02	C15	122.66
C16	132.03	C16	132.51	C16	132.57	C16	132.62	C16	132.71
C17	125.25	C17	125.96	C17	125.87	C17	125.98	C17	126.07
C18	131.64	C18	131.57	C18	131.46	C18	131.51	C18	131.65
C19	122.62	C19	125.57	C19	125.58	C19	125.63	C19	121.95
C26	135.75								
C27	122.01								
C28	124.26								
C29	122.40								
C30	124.83								
C31	120.70								
Aliphatic Carbons									
C11	53.75	C11	54.48	C11	53.64	C11	52.26	C11	40.48
C12	156.62	C12	154.68	C12	155.80	C12	154.32	C12	154.87
C13	72.40	C13	70.03	C13	69.99	C13	70.57	C13	71.90
		C26	134.34	C26	127.33	C26	70.04	C26	72.02
		C27	112.40	C27	124.38	C27	111.60	C27	75.79
				C28	19.23			C28	4.82
Boronic Acid Ester Carbons									
C20	90.63	C20	90.77	C20	90.59	C20	90.66	C20	90.85
C21	90.94	C21	90.73	C21	90.78	C21	90.79	C21	90.82
C22	27.11	C22	26.99	C22	23.85	C22	23.86	C22	23.87
C23	23.78	C23	23.72	C23	27.02	C23	27.01	C23	26.99
C24	26.83	C24	26.94	C24	27.03	C24	25.58	C24	23.84
C25	23.85	C25	23.86	C25	23.91	C25	25.65	C25	27.17

has lower values in diboronic acid derivatives (2′,3′,4′,5′ and 6′). The lowest unoccupied molecular orbital energy (E_{LUMO}) of (2)-(6) complexes is higher than (2′)-(6′) complexes. The energy of HOMO is related to the ionization energy, and the energy of LUMO is related to electron affinity. The HOMO–LUMO gap, or the energy difference between HOMO and LUMO, is a very important stability factor. A significant HOMO-LUMO gap indicates that the molecule will be stable in chemical processes [34,35]. From the table, the change in ΔE energy has higher values in diboronic acid derived compounds (2′)-(6′) compared to their counterparts. In Fig. 3, contour diagrams giving the frontier molecular orbital energies of complexes (2) and (2′) are imagined.

When the contour diagrams of the complexes are examined, the energy of HOMO is related to the ionization energy, while the energy of LUMO is related to electron affinity. The HOMO-LUMO gap or the energy difference between HOMO and LUMO is a very important stability factor. As can be seen from Fig. 3, the HOMO molecular orbitals have a hybrid appearance on the ferrocene unit, with both π molecular and d orbitals contributing. LUMO molecular orbitals represent π^* molecular orbitals. So the HOMO→LUMO transition corresponds to the $\pi \rightarrow \pi^*$ and d→π^* transitions [36].

Looking at the table of our compounds, in molecules containing boronic acid derivatives, both ionization energy and electron affinity have high values ((2)-(6)). The molecule with the lowest global hardness (and therefore the highest global softness) is said to have better activity [31,34]. Because a soft molecule is more reactive than a hard molecule [37]. When Table 5 is examined, it is seen that the diboronic acid derivatives of molecules with low hardness values are bound. The softness value is lower in monoboronic acid derivatives. According to the density functional theory, Mulliken electronegativity is the inverse of the chemical potential. Therefore, Sanderson's approach is a parameter that provides very useful information as it resembles a macroscopic thermodynamic process known as chemical potential equalization. The electronegativity or chemical potential of atoms should equalize when they interact [38]. It can be said that low electronegativity and high chemical potential increase activity. Therefore, compounds ((2′)-(6′)) are more reactive in terms of both electronegativity and chemical potential. Quantum chemical parameters such as electron-donating force and electron-accepting strength can reveal a lot about a compound's electron-donating and accepting capacities. Soft and polarizable compounds can be considered good inhibitors when the Principles of Maximum Hardness and Minimum Polarizability are studied with parallel methods [39,40]. In general, from the results obtained, mono-substituted boronic acid derivatives ((2)-(6)) are less reactive than hypothetical di-substituted boronic acid derivatives ((2′)-(6′)).

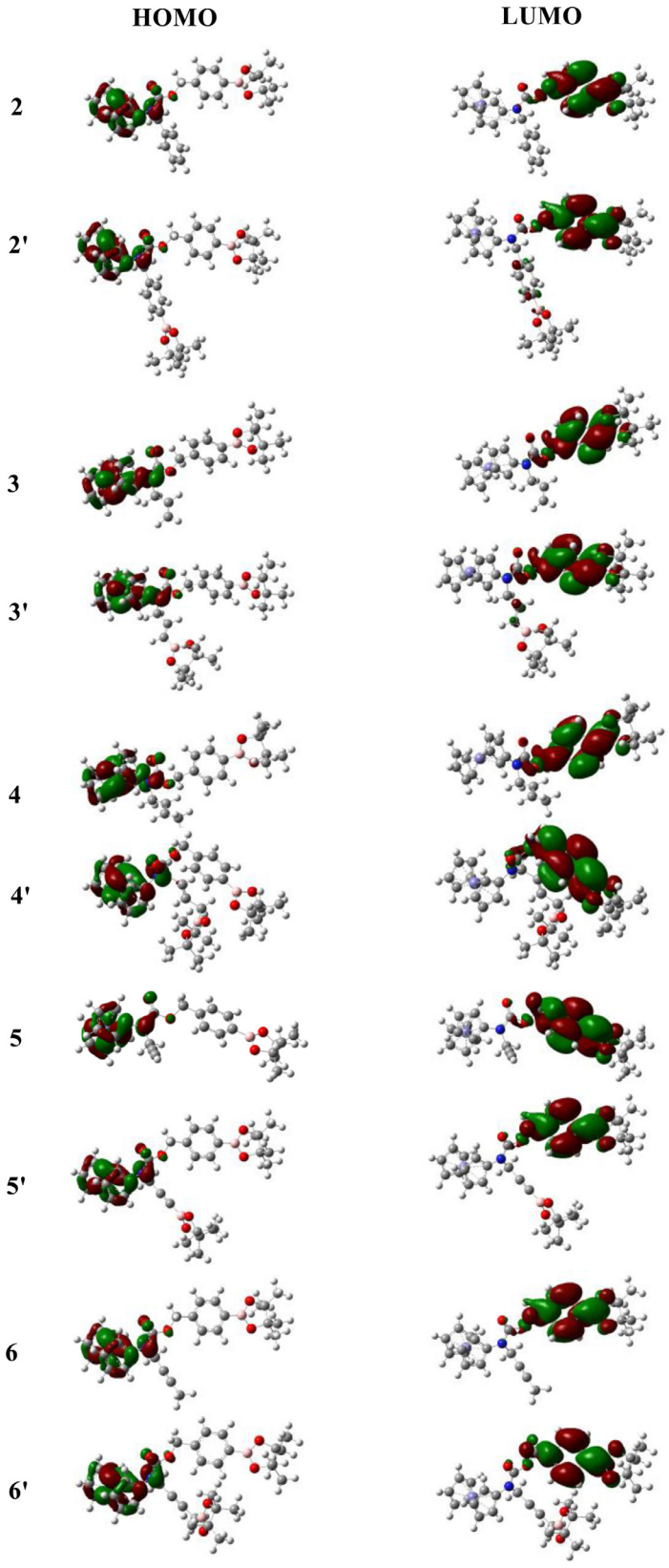

Fig. 3. Frontier molecular orbitals diagrams of complexes.

Table 4
^{13C}NMR chemical shift values (ppm) of (2′)-(6′) complexes.

(2′)	δ	(3′)	δ	(4′)	δ	(5′)	δ	(6′)	δ
Ferrocene Carbons									
C1	65.49	C1	66.93	C1	68.68	C1	67.02	C1	66.25
C2	101.16	C2	101.93	C2	101.10	C2	100.91	C2	101.09
C3	59.49	C3	58.58	C3	58.09	C3	58.60	C3	59.14
C4	64.63	C4	64.52	C4	64.14	C4	64.86	C4	64.49
C5	66.31	C5	65.66	C5	65.61	C5	66.36	C5	66.45
C6	69.37	C6	68.66	C6	69.36	C6	69.61	C6	69.59
C7	69.37	C7	69.36	C7	68.38	C7	68.63	C7	68.53
C8	69.56	C8	69.42	C8	68.96	C8	68.77	C8	69.22
C9	70.46	C9	70.33	C9	70.16	C9	70.07	C9	70.20
C10	71.41	C10	70.88	C10	71.33	C10	70.68	C10	71.13
Aromatic Carbons									
C14	135.39	C14	135.91	C14	136.31	C14	135.82	C14	137.54
C15	122.41	C15	126.93	C15	125.86	C15	122.67	C15	122.40
C16	132.21	C16	132.44	C16	131.59	C16	132.40	C16	134.10
C17	124.89	C17	125.81	C17	126.82	C17	124.73	C17	123.11
C18	131.51	C18	131.69	C18	132.47	C18	131.42	C18	130.86
C19	121.79	C19	125.87	C19	125.66	C19	121.61	C19	119.51
C26	139.31								
C27	121.17								
C28	132.60								
C29	124.06								
C30	132.93								
C31	119.64								
Aliphatic Carbons									
C11	54.16	C11	56.05	C11	53.88	C11	40.65	C11	40.64
C12	156.59	C12	155.68	C12	155.75	C12	154.79	C12	155.15
C13	71.99	C13	70.25	C13	69.91	C13	71.51	C13	67.72
		C26	150.68	C26	123.80	C26	97.52	C26	70.62
		C27	117.95	C27	128.04	C27	78.58	C27	77.61
				C28	17.72			C28	4.22
Boronic Acid Ester Carbons									
C20	91.00	C20	90.57	C20	91.28	C20	90.95	C20	90.21
C21	90.66	C21	90.62	C21	91.14	C21	90.61	C21	90.64
C22	23.78	C22	27.02	C22	23.68	C22	26.85	C22	24.08
C23	26.83	C23	23.74	C23	26.89	C23	23.91	C23	27.19
C24	27.22	C24	26.96	C24	26.44	C24	23.88	C24	23.89
C25	23.84	C25	23.92	C25	23.50	C25	27.24	C25	26.95
C32	90.84	C28	90.32	C29	89.90	C28	91.07	C29	93.03
C33	91.23	C29	89.98	C30	90.94	C29	91.11	C30	91.51
C34	26.93	C30	23.70	C31	23.66	C30	26.67	C31	26.89
C35	23.75	C31	26.89	C32	25.38	C31	23.66	C32	23.73
C36	23.85	C32	26.63	C33	22.87	C32	26.79	C33	26.47
C37	26.98	C33	23.58	C34	26.68	C33	23.59	C34	23.41

3.5. NLO properties

Metal coordination compounds with nonlinear optical (NLO) properties have been investigated for modern communication technology products in recent years. A systematic study of the electronic structure and nonlinear properties of metal complexes is of great importance in this regard. DFT studies developed with computational chemistry techniques can reveal the NLO properties of complexes [41].

Total static dipole moment (μ), mean linear polarizability (α), polarizability anisotropy ($\Delta\alpha$) and first hyperpolarizability (β) of complexes including standard urea were used to predict NLO properties, and these numerical values are given in Table 6.

$$\mu = \left(\mu_x^2 + \mu_y^2 + \mu_z^2\right)^{1/2} \tag{9}$$

$$a = \frac{1}{3}(a_{xx} + a_{yy} + a_{zz}) \tag{10}$$

$$\Delta a = \frac{1}{\sqrt{2}}\left[(a_{xx} - a_{yy})^2 + (a_{yy} - a_{zz})^2 + (a_{zz} - a_{xx})^2 + 6a_{xz}^2 + 6a_{xy}^2 + 6a_{yz}^2\right]^{1/2} \tag{11}$$

$$\beta = \left[(\beta_{xxx} + \beta_{xyy} + \beta_{xzz})^2 + (\beta_{yyy} + \beta_{yzz} + \beta_{yxx})^2 + (\beta_{zzz} + \beta_{zxx} + \beta_{zyy})^2\right]^{1/2} \tag{12}$$

The total static dipole moment(μ), mean linear polarization (α), polarization anisotropy ($\Delta\alpha$) and first hyperpolarization (β) values given in Table 6 are the basic parameters for estimating the NLO properties. According to the obtained data, the investigated complexes are superior in terms of all parameters producing standard substances. Increasing values of total static dipole moment(μ), mean linear polarization (α), polarization anisotropy ($\Delta\alpha$) and first hyperpolarization (β) parameters provide superiority in terms of NLO significance. In accordance with the parameters examined in Table 6, dipole moment (μ), mean linear polarization (α), polarization anisotropy ($\Delta\alpha$) and first hyperpolarization (β) values (2′)-(6′) of (2)-(6) complexes. higher than their complexes. This may be

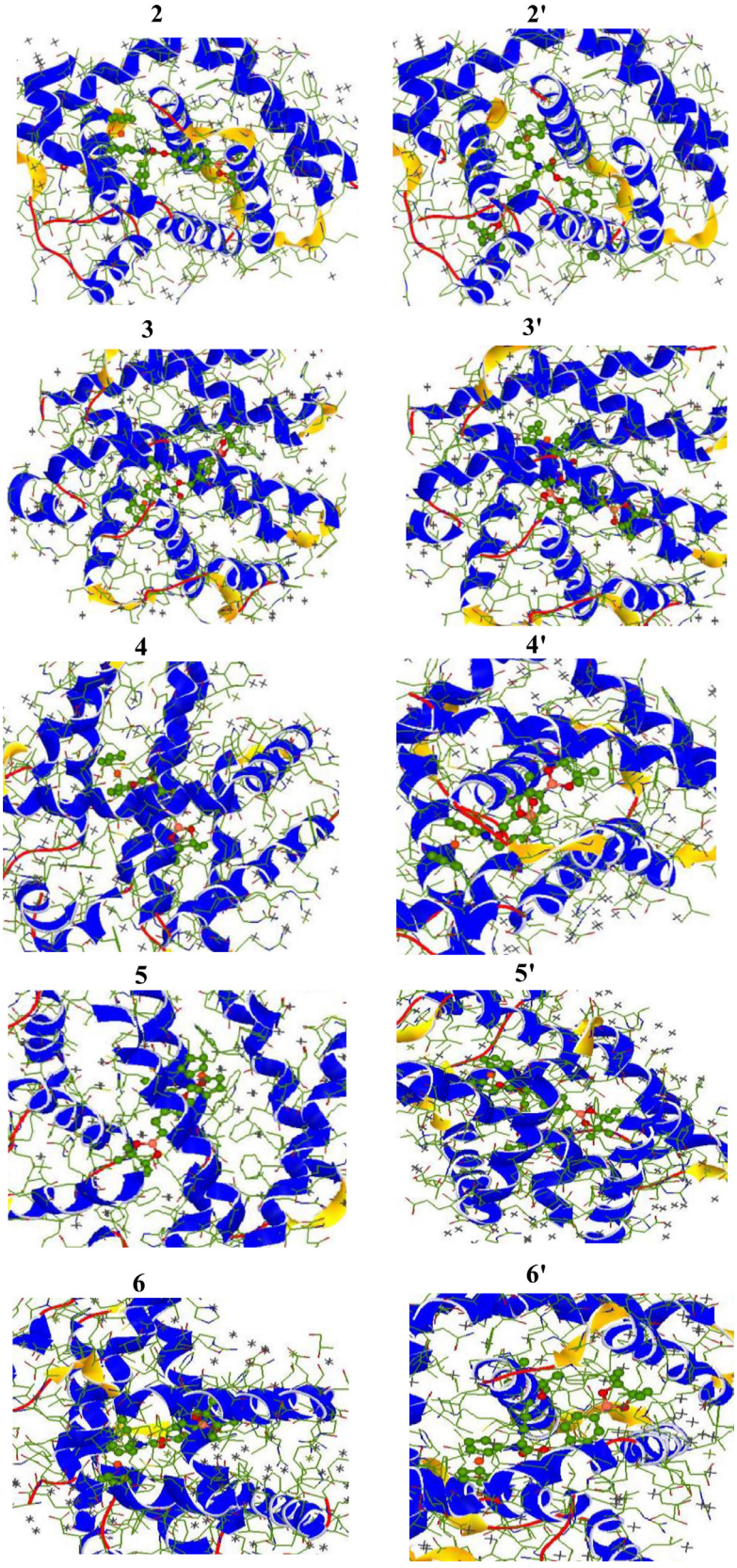

Fig. 4. The interaction modes of complexes and target protein.

Table 5
The calculated quantum chemical descriptors for the investigated complexes.

Parameters	(2)	(2′)	(3)	(3′)	(4)	(4′)	(5)	(5′)	(6)	(6′)
E_{HOMO} **(eV)**	−5.2083	−5.1512	−5.1893	−5.1403	−5.1675	−5.1702	−5.3580	−5.2301	−5.4396	−5.1566
E_{LUMO} **(eV)**	−0.7891	−0.7973	−0.8681	−0.8463	−0.8463	−0.8599	−0.8082	−0.7157	−0.7701	−0.5578
IE	5.2083	5.1512	5.1893	5.1403	5.1675	5.1702	5.3580	5.2301	5.4396	5.1566
EA	0.7891	0.7973	0.8681	0.8463	0.8463	0.8599	0.8082	0.7157	0.7701	0.5578
Δ*E*	4.4192	4.3539	4.3212	4.2940	4.3212	4.3103	4.5498	4.5144	4.6695	−4.5988
η (eV)	2.2096	2.1769	2.1606	2.1470	2.1606	2.1552	2.2749	2.2572	2.3348	2.2994
σ (eV^{-1})	0.4526	0.4594	0.4628	0.4658	0.4628	0.4640	0.4396	0.4430	0.4283	0.4349
χ (eV)	2.9987	2.9742	3.0287	2.9933	3.0069	3.0150	3.0831	2.9729	3.1048	2.8572
μ (eV^{-1})	−2.9987	−2.9742	−3.0287	−2.9933	−3.0069	−3.0150	−3.0831	−2.9729	−3.1048	−2.8572
ω	2.0348	2.0318	2.1227	2.0866	2.0923	2.0892	2.0667	1.9577	2.0645	1.7752
ε	0.4914	0.4922	0.4711	0.4793	0.4779	0.4787	0.4839	0.5108	0.4844	0.5633
ω^+	0.7939	0.7755	0.7315	0.7070	0.7183	0.7065	0.7014	0.6503	0.6901	0.5654
ω^-	3.8104	3.7910	3.9071	3.8516	3.8658	3.9151	3.860	3.7263	3.9087	3.4912
α	359.538	447.763	322.916	403.149	335.034	403.395	319.562	405.670	333.429	410.567
DM (Debye)	4.641	5.969	3.600	5.548	3.922	4.716	4.363	5.709	4.770	5.606

Table 6
The calculated total static dipole moment(μ), the average linear polarizability (α), the anisotropy of the polarizability ($\Delta\alpha$), first hyperpolarizability (β).

Parameters	μ[a]	α[b]	$\Delta\alpha$[b]	β[c]
Urea	1.9645	4.2580	9.4102	$6.67x10^{-28}$
(2)	11.2562	40.5826	101.3601	$1.94x10^{-25}$
(2′)	10.3265	40.2365	100.0130	$1.88x10^{-25}$
(3)	11.5865	41.5842	103.3654	$2.80x10^{-25}$
(3′)	10.9809	40.8854	102.9684	$2.55x10^{-25}$
(4)	12.0825	41.9995	105.0148	$2.97x10^{-25}$
(4′)	11.5942	41.3512	104.5239	$2.85x10^{-25}$
(5)	11.1563	38.1405	101.2635	$4.86x10^{-26}$
(5′)	10.2230	37.2591	100.3014	$4.08x10^{-26}$
(6)	11.0603	37.5632	100.8963	$4.51x10^{-26}$
(6′)	10.1095	37.0070	100.0025	$4.25x10^{-26}$

[a] In Debye,.
[b] In $Å^3$,.
[c] In cm^5/esu,[d]eV.

Table 7
The reorganization energies, adiabatic/vertical ionization potentials and electron affinities (all in eV) of (2)-(6) and (2′)-(6′).

	$\lambda_{e\ (eV)}$	$\lambda_{h\ (eV)}$	IPa	IPv	EAa	EAv
(2)	0.152	0.205	4.253	4.024	0.894	0.985
(2′)	0.143	0.221	5.036	4.101	0.865	0.968
(3)	0.114	0.223	5.907	4.163	0.756	0.865
(3′)	0.121	0.255	5.980	4.240	0.741	0.806
(4)	0.159	0.209	4.525	5.045	0.793	0.901
(4′)	0.136	0.211	4.727	5.162	0.785	0.899
(5)	0.254	0.256	6.654	5.485	0.623	0.772
(5′)	0.263	0.262	6.778	6.624	0.614	0.761
(6′)	0.221	0.285	6.982	6.851	0.609	0.752
(6′)	0.195	0.293	6.993	6.995	0.684	0.685

Table 8
Binding energies of all complexes and 2WH6.

Complexes	Binding Energies (kcal/mol)
(2)	−301.53
(2′)	−338.06
(3)	−315.06
(3′)	−323.73
(4)	−296.06
(4′)	−307.85
(5)	−301.27
(5′)	−340.18
(6′)	−307.00
(6′)	−312.48

due to the increase in the aliphatic groups of the complexes. It can therefore be envisaged that hypothetical complexes to which the boron substituent is added do not provide an advantage in terms of nonlinear optical properties.

3.6. Light emitting properties

DFT application of Marcus theorem was performed to predict the basic optical and electrical properties of (2)-(6) and (2′)-(6′) complexes. DFT-B3LYP/GEN level was used to make theoretical calculations on the Organic Light Emitting Diode (OLED) properties of the complexes [42].

The electron transport layer (ETL), a hole transport layer (HTL) between the cathode and an anode, and in addition to these layers, the electron injection layer adjacent to the cathode (EIL) and the hole injection layer adjacent to the anode (HIL) are a crucial factor in the performance of OLEDs. These parameters were calculated according to the equations given below and the corresponding values for the complexes examined in Table 7 are given.

$$\lambda_e = \left(E_0^- - E_-^-\right) + \left(E_-^0 - E_0^0\right) \quad (13)$$

$$\lambda_h = \left(E_0^+ - E_+^+\right) + \left(E_+^0 - E_0^0\right) \quad (14)$$

Where E_0^+ and E_0^- are the energies of the cation and anion of neutral molecule. E_+^+ and E_-^- are the energies of the cation and anion obtained from cation and anion. E_+^0 and E_-^0 are the energy of the neutral molecule calculated at the cationic and anionic state. E_0^0 is the energy of the neutral molecule at the ground state [43].

Another parameter are adiabatic/vertical ionization potentials (IPa/IPv) and adiabatic/vertical electron affinities (EAa/EAv) [44]. These parameters are obtained from Eqs. (15)-(18).

$$IPa = E_+^+ - E_0^0 \quad (15)$$

$$IPv = E_0^+ - E_0^0 \quad (16)$$

$$EAa = E_0^0 - E_-^- \quad (17)$$

$$EAv = E_0^0 - E_0^- \quad (18)$$

Here E_0^-andE_0^+ are the energy of the re-optimized anion (cation). E_-^- (E_+^+)is the energy of the anion (cation) calculated with the optimized anion (cation) structure, E_-^0 (E_+^0) is the energy of the neutral molecule calculated at the anionic (cationic) state. In addition, $E_0^0$is defined as the energy of the neutral molecule at the ground state [45].

The reference material for ETL compounds is tris(8-hydroxyquinoline) aluminum complex (Alq3) [46], while the reference material for HTL compounds is N,N'-diphenyl-N,N'-.bis(3-methylphenyl)−1,1′-diphenyl-4,4′-diamine (TPD) [47]. A good OLED material should have parameters superior to reference materials.

According to OLED implementations of DFT calculations, lower reorganization energy from reference materials indicates a higher charge transfer rate. With this approach, the suitability of ETL and HTL material can be suggested. The λe values of all examined complexes are lower than the reference Alq3 (λe= 0.276 eV) [46]. Therefore, it can be said that all complexes are more advantageous as ETL materials instead of Alq3. For the HTL material, the λh values of all the complexes are less than the λh value of the TPD (λh = 0.290 eV) [47]. For the HTL material, the studied complexes are suitable. However, boranic acid and its alkyl substituent have created a disadvantage for OLED materials. This state complies with NLO specifications. Three coordinated boron is electron deficient with empty pz orbital. Due to its strong π-acceptor character, significant delocalization occurs when conjugated with an adjacent organic π system. The presence of the vacant pz orbital predisposes boron compounds to nucleophiles, resulting in either bond cleavage or the formation of a four-coordinate borate species that causes interruption in conjugation with adjacent π [48]. Hole injection capacity can be correlated with IP and EA values. In general, molecules with smaller IP and larger EAs allow easier injection of holes from the hole (electron) transport layer to the emitter layers. (2) complex is more advantageous than the others in this regard. When the results are examined, the IP values of (2) are lower than the others. Again, the EA values of (2) are higher than the others. The order of advantage of the compounds studied as HIL and EIL compounds are almost similar to the order of NLO properties. As a result, ferrocene complexes derived from biboronic acid are not more advantageous.

3.7. Molecular docking

Molecular docking studies predict the activity between chemical species and biological macromolecules. It is also a pioneering technique for developing new drug candidate molecules. Determining the interaction energy between the protein whose crystal structure is selected and the chemical species studied allows for predicting the strength of biological activity. In this investigation, ferrocene complexes were docked with the virally encoded homolog of Bcl-2 (PDB ID: 2WH6). This protein is associated with affecting the B cell compartment such as Burkitt's lymphoma [49]. HEX 8.0.8 was used for docking [50]. This program, Spherical Polar Fourier (SPF) approximation allows the effect of rotations and translations to be calculated directly from the original expansion coefficients [26]. The coupling poses of the amino ferrocene complexes against the PDB ID: 2WH6 target protein are presented in Fig. 4. In addition, the binding energies between the complexes and the target protein are listed in Table 8.

The binding energies obtained as a result of the binding of aminoferrocene complexes to the 2WH6 target protein are given in Table 4.8. In terms of target protein representing Burkitt's lymphoma and molecules with the highest binding energies, the binding energy of complex (2) is −301.53 kcal/mol, while the binding energy of (2′) complex is −338.06 kcal/mol. The binding energy of complex (5) is −301.27 kcal/mol, the binding energy of complex (5′) is −340.18 kcal/mol. The coupling energy of ferrocene complexes containing diboranic acid ((2′)-(6′)) is higher than ferrocene complexes containing monoboranic acid. When the binding energies were examined, it was observed that the binding energies of the complexes containing diboranic acid substitution were higher than the complexes containing monobromic acid. This situation is quite similar to the order of activity obtained from quantum chemical parameters. Also, as can be seen in Fig. 4, each of the complexes bound to different regions of the 2WH6 target protein.

4. Conclusions

Computational chemistry methods ferrocene boranic acids ((2), (3), (4), (5), (6)) and their hypothetical complexes ((2′), (3′), (4′), (5′))), (6′)) were examined. In this way, ferrocene complexes, which are very difficult to optimize, have been brought to the literature. The structures of the studied complexes are proposed in three dimensions. As a result of the optimization, it was observed that the pentahapto cyclopentadienyl ligand was in a coincident position around the iron atom. Some bond lengths and bond angles obtained are suggested. In IR spectra, bond stretching modes are labeled according to the atoms of interest. Experimental and calculated NMR chemical shifts were found to be compatible with each other. According to the quantum chemical parameters, the activity of the hypothetical (2′), (3′), (4′), (5′), (6′) complexes was estimated to be higher in general. When NLO and OLED properties are examined, all of the Complexes are more advantageous than the relevant reference materials. In addition, for both properties, it was calculated that the diboranic and alkyl substituents of molecular sized complexes reduce the optical properties. The molecular docking results are quite similar to the general trend obtained with quantum chemical parameters. According to the results of the molecular dimension DFT analysis of the complex, it is estimated that the diboronic acid substituents provide advantages in terms of biological activity (Table 2).

CRediT authorship contribution statement

Sultan ERKAN: Writing, Research, Reviewing and Editing. **Usman Muhammed SANI:** Tabulation. **Savaş KAYA:** Visualization and Methodology.

Declaration of Competing Interest

The authors declare the following financial interests/personal relationships which may be considered as potential competing interests:

Sultan ERKAN reports financial support was provided by Cumhuriyet University. Sultan ERKAN reports a relationship with Cumhuriyet University that includes: employment. Sultan ERKAN has patent issued to no. Sultan Erkan reports equipment, drugs, or supplies was provided by Cumhuriyet University. Sultan Erkan reports a relationship with Cumhuriyet University that includes: speaking and lecture fees. Co-aothor- Sivas Cumhuriyet University

Data availability

Data will be made available on request.

Acknowledgments

The numerical calculations reported in this paper were performed at TUBITAK ULAKBIM, High Performance and Grid Computing Center (TRUBA Resources). Also, this paper was produced from the thesis of Usman Muhammad SANI.

Supplementary materials

Supplementary material associated with this article can be found, in the online version, at doi:10.1016/j.molstruc.2023.135312.

References

[1] N. Chavain, C. Biot, Organometallic complexes: new tools for chemotherapy, Curr. Med. Chem. 17 (25) (2010) 2729–2745.
[2] M.F. Fouda, M.M. Abd-Elzaher, R.A. Abdelsamaia, A.A. Labib, On the medicinal chemistry of ferrocene, Appl. Organomet. Chem. 21 (8) (2007) 613–625.
[3] F.A. Larik, A. Saeed, T.A. Fattah, U. Muqadar, P.A. Channar, Recent advances in the synthesis, biological activities and various applications of ferrocene derivatives, Appl. Organomet. Chem. 31 (8) (2017) e3664.
[4] S Top, Chemistry 9 (2003) 5223–5236.
[5] S. Kaur, M. Kaur, P. Kaur, K. Clays, K. Singh, Ferrocene chromophores continue to inspire. Fine-tuning and switching of the second-order nonlinear optical response, Coord. Chem. Rev. 343 (2017) 185–219.
[6] G. Gong, Y. Cao, F. Wang, G. Zhao, Planar chiral ferrocene cyclopalladated derivatives induce caspase-dependent apoptosis and antimetastasis in cancer cells, Organometallics 37 (7) (2018) 1103–1113.
[7] V. Alain, A. Fort, M. Barzoukas, C.T. Chen, M. Blanchard-Desce, S.R. Marderm, J.W. Perryr, The linear and non-linear optical properties of some conjugated ferrocene compounds with potent heterocyclic acceptors, Inorganica Chim Acta 242 (1–2) (1996) 43–49.
[8] S. Prabu, N. Palanisami, Aggregation induced emission (AIE)-active ferrocene conjugated linear $\pi-$ extended multi donor$-\pi-$ acceptor (DD′-π-A) chromophores: synthesis, structural, theoretical, linear and nonlinear optical studies, Dyes Pigm. 201 (2022) 110193.
[9] F. Limosani, F. Tessore, G. Di Carlo, A. Forni, P. Tagliatesta, Nonlinear optical properties of porphyrin, fullerene and ferrocene hybrid materials, Materials (Basel) 14 (16) (2021) 4404.
[10] R. Teimuri-Mofrad, K. Rahimpour, R. Ghadari, S. Ahmadi-Kandjani, Ferrocene based nonlinear optical chromophores: synthesis, characterization and study of optical properties, J. Mol. Liq. 244 (2017) 322–329.
[11] Y.W. Chang, M.J. Huang, C.C. Lai, C.C. Chang, M.P. Huang, C.Y. Liao, C.H. Cheng, A versatile ferrocene-containing material as a p-type charge generation layer for high-performance full color tandem OLEDs, Chem. Commun. 52 (99) (2016) 14294–14297.
[12] D.J. Young, S.W. Chien, T.A. Hor, 1, 1'-Bis (diphenylphosphino) ferrocene in functional molecular materials, Dalton Trans. 41 (41) (2012) 12655–12665.
[13] A. Irfan, Exploring the optoelectronic and charge transfer nature of ferrocene derivatives: a first-principles approach, Russ. J. Inorg. Chem. 64 (10) (2019) 1249–1256.
[14] H. Maslah, C. Skarbek, S. Pethe, R. Labruère, Anticancer boron-containing prodrugs responsive to oxidative stress from the tumor microenvironment, Eur. J. Med. Chem. (2020) 112670.
[15] R.C. Kane, P.F. Bross, A.T. Farrell, R. Pazdur, Velcade®: US FDA approval for the treatment of multiple myeloma progressing on prior therapy, Oncologist 8 (6) (2003) 508–513.
[16] R.C. Kane, R. Dagher, A. Farrell, C.W. Ko, R. Sridhara, R. Justice, R. Pazdur, Bortezomib for the treatment of mantle cell lymphoma, Clin. Cancer Res. 13 (18) (2007) 5291–5294.
[17] T.C. Kouroukis, F.G. Baldassarre, A.E. Haynes, K. Imrie, D.E. Reece, M.C. Cheung, Bortezomib in multiple myeloma: systematic review and clinical considerations, Curr. Oncol. 21 (4) (2014) e573.
[18] Z. Huang, S. Wang, R.D. Dewhurst, N.V. Ignat'ev, M. Finze, H. Braunschweig, Boron: its role in energy-related processes and applications, Angew. Chem. Int. Ed. 59 (23) (2020) 8800–8816.
[19] M. Saleem, L. Wang, H. Yu, M. Akram, R.S. Ullah, Synthesis of amphiphilic block copolymers containing ferrocene–boronic acid and their micellization, redox-responsive properties and glucose sensing, Colloid. Polym. Sci. 295 (6) (2017) 995–1006.
[20] S. Daum, S. Babiy, H. Konovalova, W. Hofer, A. Shtemenko, N. Shtemenko, A. Mokhir, Tuning the structure of aminoferrocene-based anticancer prodrugs to prevent their aggregation in aqueous solution, J. Inorg. Biochem. 178 (2018) 9–17.
[21] R. Dennington, T. Keith, J. Millam, Semichem Inc., Shawnee Mission Ks. GaussView, Version, 5 2009.
[22] M.J. Frisch, G.W. Trucks, H.B. Schlegel, G.E. Scuseria, M.A. Robb, J.R. Cheeseman, D.J. Fox, in: Gaussian 09, Revision d. 01, Gaussian. Inc., Wallingford CT, 2009, p. 201.
[23] Y. Yang, M.N. Weaver, K.M. Merz Jr., J. Phys. Chem. A 113 (36) (2009) 9843.
[24] N. Özkan, S. Erkan, K. Sayın, D. Karakaş, Research on structural, spectral (IR, UV–Vis, 1H-and 13C-NMR) and light emitting properties of triisocyano-based trinuclear Au (I) complexes, Chem. Pap. 74 (8) (2020) 2415–2425.
[25] J.A. Bohmann, F. Weinhold, T.C. Farrar, Natural chemical shielding analysis of nuclear magnetic resonance shielding tensors from gauge-including atomic orbital calculations, J. Chem. Phys. 107 (4) (1997) 1173–1184.
[26] Ritchie, D., & Orpailleur, T. (2013). Hex 8.0. 0 user manual. protein docking using spherical polar fourier correlations copyright c.
[27] D. Dechtrirat, N. Gajovic-Eichelmann, F. Wojcik, L. Hartmann, F.F. Bier, F.W. Scheller, Electrochemical displacement sensor based on ferrocene boronic acid tracer and immobilized glycan for saccharide binding proteins and E. coli, Biosens. Bioelectron. 58 (2014) 1–8.
[28] K. Lacina, M. Konhefr, J. Novotný, D. Potěšil, Z. Zdráhal, P. Skládal, Combining ferrocene, thiophene and a boronic acid: a hybrid ligand for reagentless electrochemical sensing of cis-diols, Tetrahedron Lett. 55 (21) (2014) 3235–3238.
[29] M.F. Pill, A. Kersch, H. Clausen-Schaumann, M.K. Beyer, Force dependence of the infrared spectra of polypropylene calculated with density functional theory, Polym. Degrad. Stab. 128 (2016) 294–299.
[30] S. Erkan, D. Karakaş, A theoretical study on cyclometalated iridium (III) complexes by using a density functional theory, J. Theor. Comput. Chem. 19 (02) (2020) 2050006.
[31] S. Erkan, S. Kaya, K. Sayin, D. Karakaş, Structural, spectral characterization and molecular docking analyses of mer-ruthenium (II) complexes containing the bidentate chelating ligands, Spectrochim. Acta Part A 224 (2020) 117399.
[32] K. Sayin, S.E. Kariper, T.A. Sayin, D. Karakaş, Theoretical spectroscopic study of seven zinc (II) complex with macrocyclic Schiff-base ligand, Spectrochim. Acta Part A 133 (2014) 348–356.
[33] R.T. Sanderson, Principles of electronegativity Part I. General nature, J. Chem. Educ. 65 (2) (1988) 112.
[34] R. Junejo, N. Shams Jalbani, S. Kaya, S. Erkan, R. Marzouki, S. Memon, Equilibrium and computational chemical modelling studies for the removal of methyl orange and methyl red dyes from water using modified silica resin, Int. J. Environ. Anal. Chem. (2021) 1–17.
[35] S.A. Gungor, I. Sahin, O. Gungor, S.E. Kariper, F. Tumer, M. Kose, Pamoic acid esters and their xanthene derivatives: flourimetric detection of nitroaromatic compounds and non-linear optical properties, Sens. Actuators B 255 (2018) 3344–3354.
[36] K. Sayin, D. Karakaş, N. Karakuş, T.A. Sayin, Z. Zaim, S.E. Kariper, Spectroscopic investigation, FMOs and NLO analyses of Zn (II) and Ni (II) phenanthroline complexes: a DFT approach, Polyhedron 90 (2015) 139–146.
[37] H. Kırpık, S. Erkan, M. Kose, A new 3-substituted BODIPY dye: synthesis, crystal structure, photophysical, non-linear optic and OLED properties, J. Mol. Struct. 1252 (2022) 132090.
[38] A. Irfan, S. Muhammad, A.R. Chaudhry, A.G. Al-Sehemi, R. Jin, Tuning of optoelectronic and charge transport properties in star shaped anthracenothiophene-pyrimidine derivatives as multifunctional materials, Optik (Stuttg) 149 (2017) 321–331.
[39] H.H. Khalid, S. Erkan, N. Bulut, Halogens effect on spectroscopy, anticancer and molecular docking studies for platinum complexes, Optik (Stuttg) (2021) 166324.
[40] M. Cölle, J. Gmeiner, W. Milius, H. Hillebrecht, W. Brütting, Preparation and characterization of blue-luminescent tris (8-hydroxyquinoline)-aluminum (Alq3), Adv. Funct. Mater. 13 (2) (2003) 108–112.
[41] A.H. Pandith, N. Islam, Electron transport and nonlinear optical properties of substituted aryldimesityl boranes: a DFT study, PLoS One 9 (12) (2014) e114125.
[42] A. Üngördü, Charge transfer properties of Gaq3 and its derivatives: an OLED study, Chem. Phys. Lett. 733 (2019) 136696.
[43] A. Üngördü, Optoelectronic and electric properties of 8-hydroxyquinoline-based complexes with divalent metal ions, Mater. Chem. Phys. 281 (2022) 125899.
[44] R.R. Valiev, B.F. Minaev, R.M. Gadirov, E.N. Nikonova, T.A. Solodova, S.Y. Nikonov, … T.N. Kopylova, Electroluminescence of halogen complexes with monovalent copper: OLED devices and DFT modeling, Russ. Phys. J. 58 (9) (2016) 1205–1211.
[45] S. Vijayalakshmi, S. Kalyanaraman, DFT and TD-DFT approach for the analysis of NLO and OLED applications of 9-anthraldehyde, Optik (Stuttg) 125 (10) (2014) 2429–2432.
[46] C.Y. Kwong, A.B. Djurišić, W.C.H. Choy, D. Li, M.H. Xie, W.K. Chan, P.C. Chui, Efficiency and stability of different tris (8-hydroxyquinoline) aluminum (Alq3) derivatives in OLED applications, Mater. Sci. Eng. B Solid State Mater. Adv. Technol. 116 (1) (2005) 75–81.
[47] H. Xin, M. Guang, F.Y. Li, Z.Q. Bian, C.H. Huang, K. Ibrahim, F.Q. Liu, Photoluminescence and electroluminescence of the exciplex formed between a terbium ternary complex and N, N′-diphenyl-N, N′-bis (3-methylphenyl)-1, 1′-diphenyl-4, 4′-diamine, Phys. Chem. Chem. Phys. 4 (23) (2002) 5895–5898.
[48] M.G. Giuffreda, M. Bruschi, H.P. Lüthi, Electron delocalization in linearly π-conjugated systems: a concept for quantitative analysis, Chemistry 10 (22) (2004) 5671–5680.
[49] M. Kvansakul, A.H. Wei, J.I. Fletcher, S.N. Willis, L. Chen, A.W. Roberts, … P.M. Colman, Structural basis for apoptosis inhibition by Epstein-Barr virus BHRF1, PLoS Pathog. 6 (12) (2010) e1001236.
[50] M.S. Harika, T.R. Kumar, L.S.S. Reddy, Docking studies of benzimidazole derivatives using hex 8.0, Int. J. Pharm. Sci. Res. 8 (4) (2017) 1677.